Constraints on the $s - \bar{s}$ asymmetry of the proton in chiral effective theory

X. G. Wang,[1] Chueng-Ryong Ji,[2] W. Melnitchouk,[3] Y. Salamu,[4] A. W. Thomas,[1] and P. Wang[4,5]

[1] *CoEPP and CSSM, University of Adelaide, Adelaide SA 5005, Australia*
[2] *North Carolina State University, Raleigh, North Carolina 27695, USA*
[3] *Jefferson Lab, Newport News, Virginia 23606, USA*
[4] *Institute of High Energy Physics, CAS, Beijing 100049, China*
[5] *Theoretical Physics Center for Science Facilities, CAS, Beijing 100049, China*

(Dated: March 21, 2016)

We compute the $s - \bar{s}$ asymmetry in the proton in chiral effective theory, using phenomenological constraints based upon existing data. Unlike previous meson cloud model calculations, which accounted for kaon loop contributions with on-shell intermediate states alone, this work includes off-shell terms and contact interactions, which impact the shape of the $s - \bar{s}$ difference. Using a regularization procedure that preserves chiral symmetry and Lorentz invariance, we find that existing data limit the integrated value of the first moment of the asymmetry to the range $-0.07 \times 10^{-3} \leq \langle x(s-\bar{s})\rangle \leq 1.12 \times 10^{-3}$ at a scale of $Q^2 = 1$ GeV^2. In contrast to some suggestions in the literature, the magnitude of this correction is too small to account for the NuTeV anomaly.

The nature of the quark–antiquark ($q\bar{q}$) sea, which complements the three-valence quark structure of the proton, continues to puzzle and surprise us, as new generations of experiments provide deeper insights into its dynamical origins. From the early simple expectations of a featureless, virtual sea consisting of $q\bar{q}$ pairs generated by gluon radiation in perturbative quantum chromodynamics (QCD), a major paradigm shift occurred with the observation [1–4] of a predicted [5] large asymmetry between $\bar{d}$ and $\bar{u}$ quarks in the proton. This challenged our traditional view of the nucleon's peripheral structure, calling into question long held assumptions about the role of nonperturbative physics in understanding the phenomenology of parton distribution functions (PDFs).

With the realization that nonperturbative aspects of QCD were vital for understanding the 5-quark Fock state components of the nucleon light-front wave function [5–9], an obvious question to ask was whether such effects could lead to other nontrivial features in the $q\bar{q}$ sea. An asymmetry between s and $\bar{s}$ quarks in the nucleon, as anticipated by Signal and Thomas [10], was a natural consequence of SU(3) chiral symmetry breaking in QCD, and speculation later also arose about quark–antiquark asymmetries for charm and heavier quarks [11–14]. Similar considerations led to questioning the traditional expectations of flavor symmetric polarized sea quarks [15] and even the assumption of charge symmetry in the nucleon PDFs [16–18].

Apart from its intrinsic interest, the possible strange quark asymmetry, $s-\bar{s}$, is of great importance in connection with its contribution to the Paschos-Wolfenstein ratio and the NuTeV anomaly [19], which suggested a surprisingly large value for the weak mixing angle, $\sin^2\theta_W$. A positive value of the integrated difference

$$S^- \equiv \langle x(s-\bar{s})\rangle = \int_0^1 dx\, x\,(s(x) - \bar{s}(x)), \qquad (1)$$

of the order $S^- \sim 2 \times 10^{-3}$, along with other corrections such as charge symmetry violation, was found to significantly reduce the excess and bring the NuTeV $\sin^2\theta_W$ measurement closer to the standard model value [20].

Unfortunately, a reliable estimate of the strange asymmetry has been very difficult to obtain. An analysis of early ν and $\bar{\nu}$ deep-inelastic scattering (DIS) data from BEBC, CDHS and CDHSW [21] found a harder s distribution compared with $\bar{s}$, albeit with a rather large uncertainty, $S^- \approx (2 \pm 3) \times 10^{-3}$. More recent experimental information has come from dimuon production in neutrino-nucleus reactions at Fermilab by the CCFR [22] and NuTeV [23] collaborations, with an NLO analysis finding $S^- = (1.96 \pm 1.43) \times 10^{-3}$ at $Q^2 = 16$ GeV^2 [24].

On the theoretical side, calculations based upon fluctuations into meson-baryon Fock components [25–32] have led to a fairly wide range of predictions, $S^- \sim (-1 \text{ to } +9) \times 10^{-3}$, resulting from the ad hoc assumptions of those models. Clearly, if one is to make reliable predictions for S^-, a more systematic approach is needed, one which has a more direct connection to the underlying QCD theory.

In this Letter we present the first systematic chiral treatment of the $s - \bar{s}$ asymmetry guided by the need to preserve the model independent leading nonanalytic (LNA) behavior of the moments of the strange PDFs. This work builds upon the unambiguous connection between the kaon cloud of the nucleon and QCD which followed the realization [33] that in chiral expansions of moments of strange quark PDFs, the coefficients of the LNA terms in the kaon mass m_K are model independent and can only arise from pseudoscalar meson loops. Starting from the most general effective Lagrangian consistent with the chiral symmetry of QCD, at a given order in the chiral expansion a unique set of diagrams can be identified and computed systematically [34, 35]. The long distance ($m_K \to 0$) effects in such expansions are thus dictated solely by chiral symmetry and gauge invariance, while the short distance contributions are treated with a

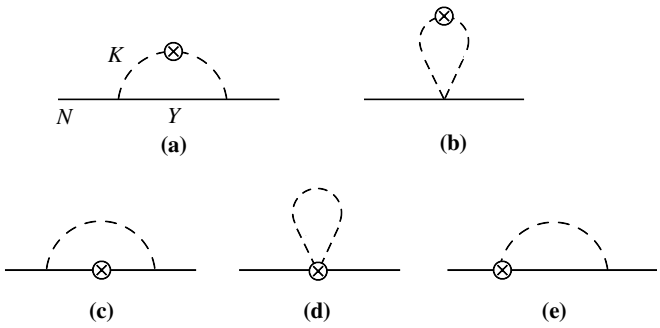

FIG. 1: Loop contributions to the $\bar{s}$ PDF from (a) kaon rainbow and (b) kaon bubble diagrams, and to the s-quark PDF from (c) hyperon rainbow, (d) tadpole, and (e) Kroll-Ruderman diagrams. Nucleons N and hyperons $Y = \Lambda, \Sigma$ are denoted by external and internal solid lines, respectively, and kaons K by dashed lines. The KR diagram with a current insertion on the right-hand vertex is not shown.

particular regularization procedure.

Expanding the chiral SU(3) Lagrangian to lowest order, the complete set of diagrams that contribute to $s - \bar{s}$ is illustrated in Fig. 1. The direct couplings to the kaon loops in Fig. 1(a) and (b) contribute to the $\bar{s}$ PDF, while the s-quark PDF contributions arise from the diagrams involving couplings to hyperons illustrated in Fig. 1(c)–(e). A general feature of the chiral effective theory constrained analyses is the presence of contact terms in Figs. 1(b) and (d) that give rise to contributions at zero kaon light-cone momentum fractions $y = k^+/p^+$, where k is the four-momentum carried by the kaon and p the four-momentum of the proton. These are typically not accounted for in model calculations, which include only the rainbow diagrams in Figs. 1(a) and (c). The Kroll-Ruderman (KR) terms represented in Fig. 1(e) are needed to preserve gauge invariance.

The loop contributions to $\bar{s}$ from the kaon rainbow and kaon bubble diagrams can be written as a standard convolution of nucleon $\to$ kaon + hyperon splitting functions, $f_{KY}^{(\rm rbw)}$ and $f_K^{(\rm bub)}$, with the $\bar{s}$ PDF in the kaon,

$$\bar{s}(x) \;=\; \left(\sum_{KY} f_{KY}^{(\rm rbw)} + \sum_K f_K^{(\rm bub)} \right) \otimes \bar{s}_K, \qquad (2)$$

where the rainbow terms are summed over $KY = K^+\Lambda$, $K^+\Sigma^0$ and $K^0\Sigma^+$, and the kaon bubble terms over $K = K^+, K^0$, and $\otimes$ denotes the convolution [36, 37]. The s-quark PDF is also a convolution,

$$s(x) \;=\; \sum_{YK} \left(\bar{f}_{YK}^{(\rm rbw)} \otimes s_Y + \bar{f}_{YK}^{(\rm KR)} \otimes s_Y^{(\rm KR)} \right) + \sum_K \bar{f}_K^{(\rm tad)} \otimes s_K^{(\rm tad)}, \qquad (3)$$

where $\bar{f}(y) \equiv f(1-y)$, with $1-y$ the hyperon momentum fraction when the kaon carries y. The hyperon rainbow contributions $f_{YK}^{(\rm rbw)}$ are again summed over all YK combinations, and $f_{YK}^{(\rm KR)}$ are the splitting functions associated with the KR diagrams. The splitting functions for the tadpole diagram, Fig. 1(d), are equal to the $f_K^{(\rm bub)}$ bubble functions from Fig. 1(b). The strange quark hyperon PDFs s_Y, $s_Y^{(\rm KR)}$ and $s_K^{(\rm tad)}$ for the rainbow, KR and tadpole diagrams, respectively, can be related to the u and d PDFs in the proton using SU(3) symmetry.

The splitting function $f_{KY}^{(\rm rbw)}$ in Eq. (2) for the kaon rainbow diagram can be written as a sum of two terms,

$$f_{KY}^{(\rm rbw)}(y) = \frac{C_{KY}^2 \overline{M}^2}{(4\pi f_P)^2} \left[f_Y^{(\rm on)}(y) + f_K^{(\delta)}(y) \right], \qquad (4)$$

where $f_Y^{(\rm on)}$ and $f_K^{(\delta)}$ are the on-shell and δ-function contributions, respectively, M (M_Y) are the nucleon (hyperon) masses, $\overline{M} = M + M_Y$, and f_P is the pseudoscalar meson decay constant. The couplings C_{KY} are given in terms of the SU(3) coefficients D and F. The on-shell hyperon piece,

$$f_Y^{(\rm on)}(y) = y \int dk_\perp^2 \, \frac{k_\perp^2 + [M_Y - (1-y)M]^2}{(1-y)^2 D_{KY}^2} F^{(\rm on)}, \qquad (5)$$

contributes at $y > 0$, where $D_{KY} \equiv -[k_\perp^2 + y M_Y^2 + (1-y) m_K^2 - y(1-y)M^2]/(1-y)$ is the kaon virtuality for an on-shell hyperon intermediate state, and $F^{(\rm on)}$ is an ultraviolet regulator function. The function $f_K^{(\delta)}$, on the other hand, arises from kaons with $y = 0$,

$$f_K^{(\delta)}(y) = \frac{1}{\overline{M}^2} \int dk_\perp^2 \, \log \Omega_K \, \delta(y) \, F^{(\delta)}, \qquad (6)$$

where $\Omega_K = k_\perp^2 + m_K^2$, and $F^{(\delta)}$ is the corresponding regulator. The K bubble diagram in Fig. 1(b) originates with the Weinberg-Tomozawa part of the chiral Lagrangian, and has a distribution, $f_K^{(\rm bub)}$, similar to the δ-function part of the rainbow contribution, but with a normalization that is independent of the SU(3) couplings,

$$f_{K^+}^{(\rm bub)} = 2 f_{K^0}^{(\rm bub)} = -\frac{\overline{M}^2}{(4\pi f_P)^2} f_K^{(\delta)}. \qquad (7)$$

For the splitting function associated with the hyperon rainbow contribution in Eq. (3) one finds

$$f_{YK}^{(\rm rbw)}(y) = \frac{C_{KY}^2 \overline{M}^2}{(4\pi f_P)^2} \left[f_Y^{(\rm on)}(y) + f_Y^{(\rm off)}(y) - f_K^{(\delta)}(y) \right], \qquad (8)$$

where the first (on-shell) and third (δ-function) terms are as in the kaon rainbow contributions, and the hyperon off-shell term is

$$f_Y^{(\rm off)}(y) = 2\overline{M} \int dk_\perp^2 \, \frac{[M_Y - (1-y)M]}{(1-y) D_{KY}} F^{(\rm off)}, \qquad (9)$$

with $F^{(\rm off)}$ the corresponding off-shell regulating function. For the KR contributions in Fig. 1(e), necessary

for the preservation of gauge symmetry [38], one has

$$f_{YK}^{(\rm KR)}(y) = \frac{C_{KY}^2 \overline{M}^2}{(4\pi f_P)^2} \left[-f_Y^{(\rm off)}(y) + 2 f_K^{(\delta)}(y) \right], \qquad (10)$$

so that the rainbow and KR contributions satisfy $f_{YK}^{(\rm rbw)} + f_{YK}^{(\rm KR)} = f_{KY}^{(\rm rbw)}$. Finally, the tadpole contribution in Fig. 1(d) is related to the bubble term in Eq. (7), $f_K^{(\rm tad)} = f_K^{(\rm bub)}$. These two conditions guarantee that the net strangeness in the nucleon is zero, $\langle s - \bar{s} \rangle = 0$.

To regulate the ultraviolet divergences in the splitting functions one introduces a regularization procedure, such as a cutoff [37] or a phenomenological form factor [39]. Physically, this takes into account the finite size of the baryon to which the chiral field couples [40, 41]. Here we adopt the Pauli-Villars (PV) method, which preserves the required symmetries and offers many of the advantages of finite range regularization. In this approach one subtracts from the point-like amplitudes expressions in which the propagator mass is replaced by a cutoff mass μ_1, so that at large momenta the difference between the amplitudes vanishes [42]. For the δ-function term, because both the k^- and $k_\perp^2$ integrations are divergent, a second subtraction, with regulator mass μ_2, is necessary to render the integrals finite.

For the valence PDFs of the mesons we use the recent fit by Aicher *et al.* [43], assuming $\bar{s}_{K^+} = \bar{s}_{K^0} = \bar{d}_{\pi^+}$. The strange quark PDFs in the hyperons are related using SU(3) symmetry to the u and d PDFs in the proton, $s_\Lambda = (2u - d)/3$ and $s_{\Sigma^+} = s_{\Sigma^0} = d$, for which we use parametrization of Martin *et al.* [44]. For the KR diagrams, the strange PDFs at the KNY vertex can be related to the spin-dependent PDFs in the proton, $s_\Lambda^{(\rm KR)} = (2\Delta u - \Delta d)/(3F + D)$ and $s_{\Sigma^+}^{(\rm KR)} = s_{\Sigma^0}^{(\rm KR)} = \Delta d/(F - D)$, and the fit from Leader *et al.* [45] is used for both the polarized PDFs and the D and F values to ensure each of the PDFs is normalized to unity. Finally, for the strange PDF at the $ppKK$ vertex of the tadpole diagram, one has $s_{K^+}^{(\rm tad)} = u/2$ and $s_{K^0}^{(\rm tad)} = d$.

With these relations, the only free parameters in the calculation are the cutoffs μ_1 and μ_2, which can be constrained phenomenologically. The ideal process for constraining μ_1 is inclusive Λ hadroproduction, $pp \to \Lambda X$. At small values of y and $k_\perp$ the K exchange contribution in Fig. 1(a) is expected to dominate, while at higher momenta heavier meson and baryon intermediate states, as well as multi meson-exchange processes, will become more important [39].

In Fig. 2 we compare the available bubble chamber data from the CERN proton synchrotron [46] for the lowest available transverse momentum bins. For the differential cross section here the current operator corresponds to the total pK^+ cross section, for which we take the constant value $\sigma_{\rm tot}^{pK^+} = 19.9 \pm 0.1$ mb [47]. We find the best fit value for the cutoff $\mu_1 = 545$ MeV, which is

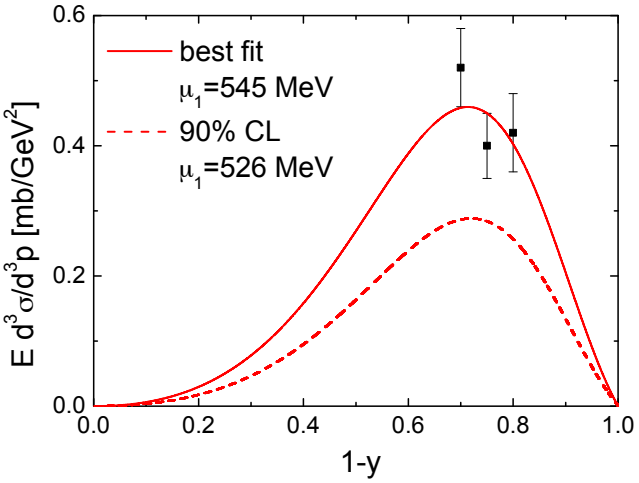

FIG. 2: Differential cross section for the best fit to the $pp \to \Lambda X$ data [46] in the region $y < 0.35$ (solid curve, $\mu_1 = 545$ MeV), as a function of $1 - y$ for $k_\perp = 75$ MeV, and for a fit 2σ (90% CL) from the central values (dashed curve, $\mu_1 = 526$ MeV).

taken to yield an upper limit on the kaon contribution. Contributions from non-kaonic backgrounds may reduce this upper limit, although at these kinematics the effect should not be large. As a conservative estimate of the impact of this uncertainty, we also consider the fit that is two standard deviations away, which corresponds to $\mu_1 = 526$ MeV. These limits yield a range of momentum fractions carried by $\bar{s}$ quarks in the nucleon from $\langle \bar{s} \rangle = 3.4 \times 10^{-3}$ to 5.7×10^{-3}.

Because the convolution in Eq. (2) transforms the $y = 0$ contribution in $f_K^{(\delta)}$ to $x = 0$, in practice the $\bar{s}$ distribution will not provide information on the cutoff μ_2. For the s-quark PDF, since the convolution in Eq. (3) is expressed in terms of the splitting functions evaluated at $1 - y$, the $f_K^{(\delta)}$ contributions here will be transformed to nonzero values of x and appear valence-like. Comparison with the x dependence of the s PDF can then constrain the value of μ_2.

Our strategy is to fix μ_1 to the maximum value allowed by the comparison with the Λ production data and obtain the corresponding maximum value for μ_2 such that the calculated $s + \bar{s}$ does not exceed the errors on the total phenomenological PDFs, $(s + \bar{s})_{\rm loops} \leq (s + \bar{s})_{\rm tot}$. This is illustrated in Fig. 3, where the individual s and $\bar{s}$ PDFs from K loops are compared with the average $(s + \bar{s})/2$ parametrization from Ref. [48].

For a fixed μ_1, the allowed range for μ_2 with the PV regularization is $m_K \leq \mu_2 \leq \mu_2^{\rm max}$. At the prefered value found in Fig. 2, $\mu_1 = 545$ MeV, the upper limit on μ_2 is $\mu_2^{\rm max} = 600$ MeV. The corresponding range for the strange asymmetry is $-0.07 \times 10^{-3} \leq S^- \leq 0.42 \times 10^{-3}$ at $Q^2 = 1$ GeV^2. Using the lower value, $\mu_1 = 526$ MeV, reduces the allowed momentum that the s quark can carry,

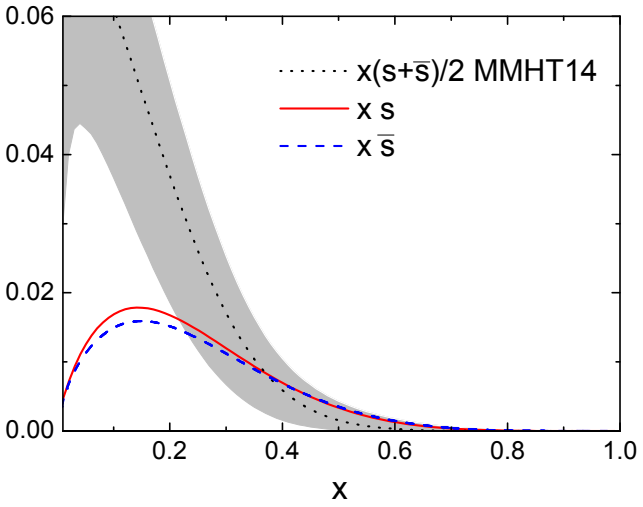

FIG. 3: Strange xs (solid red curve) and antistrange $x\bar{s}$ (dashed blue curve) PDFs from kaon loops for cutoffs $\mu_1 = 545$ MeV and $\mu_2 = 600$ MeV that give the maximum total $s+\bar{s}$, compared with the average $x(s+\bar{s})/2$ distribution from the MMHT14 global fit [48] (gray band).

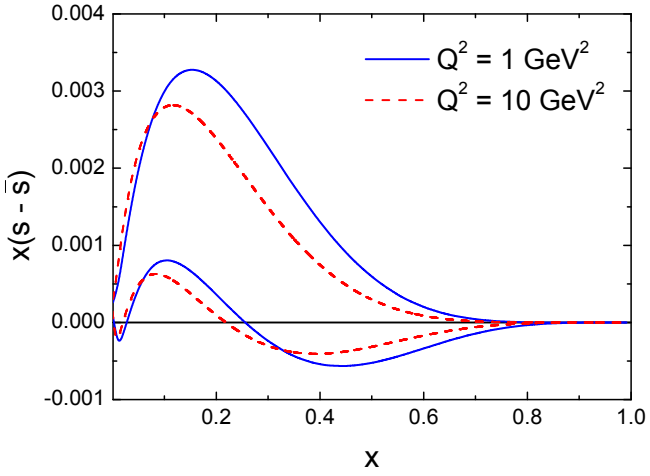

FIG. 4: Strange quark asymmetry $x(s-\bar{s})$ at $Q^2 = 1$ GeV^2 (solid blue curves) and evolved to $Q^2 = 10$ GeV^2 (dashed red curves). The upper (lower) curves correspond to the maximum (minimum) value for $S^- = 1.12 \times 10^{-3}$ (-0.07×10^{-3}), for cutoff parameters $\mu_1 = 526$ MeV, $\mu_2 = 894$ MeV ($\mu_1 = 545$ MeV, $\mu_2 = m_K$).

and consequently permits a higher upper limit on μ_2 that still satisfies the constraint in Fig. 3. The limit in this case becomes $\mu_2^{\rm max} = 894$ MeV, and the range for the strange asymmetry is $-0.01 \times 10^{-3} \leq S^- \leq 1.12 \times 10^{-3}$. Combining these limits, the strange asymmetry for the maximum allowed variations on μ_1 and μ_2 consistent with the available data lies in the range $-0.07 \times 10^{-3} \leq S^- \leq 1.12 \times 10^{-3}$.

For these extremal S^- values, the corresponding shape of $x(s-\bar{s})$ is displayed in Fig. 4. For $\mu_1 = 526$ MeV, the asymmetry remains positive for all x, peaking at $x \approx 0.15$. Interestingly, for this case there is no zero crossing at $x > 0$; conservation of strangeness is ensured by the presence of the nonzero contributions from the δ-function term $f_K^{(\delta)}$ at $x = 0$. This feature is not present in previous loop calculations based on kaon loops, which include only rainbow diagrams, nor in phenomenological PDF fits. For the parameters that give the minimal S^- value, the $x(s-\bar{s})$ distribution also peaks at $x \approx 0.1$, but has a significantly smaller magnitude. Furthermore, the distribution becomes negative for $x \gtrsim 0.2$, which leads to the strong cancelation with the positive distribution at smaller x.

To assess the impact of these asymmetries on the NuTeV anomaly and the extraction of the weak mixing angle, we fold the calculated distributions with the acceptance functional for the NuTeV data [23]. Varying the μ_1 and μ_2 parameters over their maximally allowed range, we find a correction, $\Delta(\sin^2\theta_W)$, to the weak angle from the strange asymmetry of $-7.7 \times 10^{-4} \leq \Delta(\sin^2\theta_W) \leq -6.7 \times 10^{-7}$ at $Q^2 = 10$ GeV^2. Remarkably, for all acceptable values of the cutoff parameters, the correction $\Delta(\sin^2\theta_W)$ remains negative. While this has the same sign as that needed to reduce the NuTeV discrepancy, the small numerical values that we find reduce the NuTeV anomaly by less than 0.5 σ.

We have also considered contributions to the asymmetry from kaon loops accompanied by decuplet hyperons, such as the Σ^*. Any contribution to S^- from these is tempered by the need to reduce the cut-off for the octet component so that the constraint on $s + \bar{s}$ is still respected. As a result, for the range of PV cutoffs considered here we find the net effect of the decuplet to be rather small. Inclusion of higher mass mesons, such as the strange vector K^* mesons [27, 28], goes beyond the chiral theory framework and these are more naturally treated as short-distance contributions, which should not be added incoherently to other DIS processes.

The virtue of the current analysis is that we have for the first time computed the full set of diagrams to lowest order within the effective chiral theory, revealing a small but nonzero valence-like component of the strange sea which has important phenomenological implications. With the conservative uncertainties chosen for the parameters, we believe this is the most reliable estimate to date of the chiral correction to the NuTeV extraction of $\sin^2\theta_W$ from the strange quark asymmetry. ultimately, $s - \bar{s}$ should be determined empirically and, in the absence of high precision ν and $\bar{\nu}$ data on protons, the best hope for better constraints may lie with the associated production of charm with weak bosons at the LHC [49].

We acknowledge helpful discussions with J. T. Londergan at an early stage of this work. This work was supported by the DOE Contract No. DE-AC05-06OR23177, under which Jefferson Science Associates, LLC operates Jefferson Lab, DOE Contract No. DE-FG02-03ER41260, the Australian Research Council through the ARC Centre of Excellence for Particle Physics at the Terascale (CE110001104), an ARC Australian Laureate Fellowship FL0992247 and DP151103101, and by NSFC under Grant No. 11475186, CRC 110 by DFG and NSFC.

[1] M. Arneodo *et al.*, Phys. Rev. D **50**, 1 (1994).
[2] K. Ackerstaff *et al.*, Phys. Rev. Lett. **81**, 5519 (1998).
[3] A. Baldit *et al.*, Phys. Lett. B **332**, 244 (1994).
[4] R. S. Towell *et al.*, Phys. Rev. D **64**, 052002 (2001).
[5] A. W. Thomas, Phys. Lett. B **126**, 97 (1983).
[6] J. Speth and A. W. Thomas, Adv. Nucl. Phys. **24**, 83 (1998).
[7] R. Vogt, Prog. Part. Nucl. Phys. **45**, S105 (2000).
[8] G. T. Garvey and J. C. Peng, Prog. Part. Nucl. Phys. **47**, 203 (2001).
[9] W.-C. Chang and J.-C. Peng, Phys. Rev. Lett. **106**, 252002 (2011); J.-C. Peng and J.-W. Qiu, Prog. Part. Nucl. Phys. **76**, 43 (2014).
[10] A. I. Signal and A. W. Thomas, Phys. Lett. B **191**, 205 (1987).
[11] W. Melnitchouk and A. W. Thomas, Phys. Lett. B **414**, 134 (1997).
[12] S. Paiva *et al.*, Mod. Phys. Lett. A **13**, 2715 (1998).
[13] T. J. Hobbs, J. T. Londergan and W. Melnitchouk, Phys. Rev. D **89**, 074008 (2014).
[14] F. Lyonnet *et al.*, JHEP **1507**, 141 (2015).
[15] A. I. Signal, A. W. Schreiber and A. W. Thomas, Mod. Phys. Lett. A **6**, 271 (1991).
[16] E. Sather, Phys. Lett. B **274**, 433 (1992).
[17] E. N. Rodionov, A. W. Thomas and J. T. Londergan, Mod. Phys. Lett. A **9**, 1799 (1994).
[18] J. T. Londergan, J. C. Peng and A. W. Thomas, Rev. Mod. Phys. **82**, 2009 (2010).
[19] G. P. Zeller *et al.*, Phys. Rev. Lett. **88**, 091802 (2002).
[20] W. Bentz, I. C. Cloet, J. T. Londergan and A. W. Thomas, Phys. Lett. B **693**, 462 (2010).
[21] V. Barone, C. Pascaud and F. Zomer, Eur. Phys. J. C **12**, 243 (2000).
[22] A. O. Bazarko *et al.*, Z. Phys. C **65**, 189 (1995).
[23] G. P. Zeller *et al.*, Phys. Rev. D **65**, 111103(R) (2002); 119902(E) (2003).
[24] D. Mason *et al.*, Phys. Rev. Lett. **99**, 192001 (2007).
[25] W. Melnitchouk and M. Malheiro, Phys. Rev. C **55**, 431 (1997).
[26] W. Melnitchouk and M. Malheiro, Phys. Lett. B **451**, 224 (1999).
[27] F. G. Cao and A. I. Signal, Phys. Lett. B **559**, 229 (2003).
[28] L. L. Barz *et al.*, Nucl. Phys. **A640**, 259 (1998).
[29] J. Alwall and G. Ingelman, Phys. Rev. D **70**, 111505 (2004).
[30] Y. Ding, R. G. Xu and B. Q. Ma, Phys. Lett. B **607**, 101 (2005).
[31] M. Wakamatsu, Phys. Rev. D **71**, 057504 (2005).
[32] T. J. Hobbs, M. Alberg and G. A. Miller, Phys. Rev. C **91**, 035205 (2015).
[33] A. W. Thomas, W. Melnitchouk and F. M. Steffens, Phys. Rev. Lett. **85**, 2892 (2000).
[34] J.-W. Chen and X. Ji, Phys. Rev. Lett. **87**, 152002 (2001); **88**, 249901(E) (2002).
[35] D. Arndt and M. J. Savage, Nucl. Phys. **A697**, 429 (2002).
[36] M. Burkardt *et al.*, Phys. Rev. D **87**, 056009 (2013).
[37] Y. Salamu, C.-R. Ji, W. Melnitchouk and P. Wang, Phys. Rev. Lett. **114**, 122001 (2015).
[38] C.-R. Ji, W. Melnitchouk and A. W. Thomas, Phys. Rev. D **88**, 076005 (2013).
[39] H. Holtmann, A. Szczurek and J. Speth, Nucl. Phys. **A569**, 631 (1996).
[40] J. F. Donoghue, B. R. Holstein and B. Borasoy, Phys. Rev. D **59**, 036002 (1999).
[41] R. D. Young, D. B. Leinweber and A. W. Thomas, Nucl. Phys. Proc. Suppl. **141**, 233 (2005).
[42] X. Wang *et al.*, in preparation (unpublished, 2016).
[43] M. Aicher, A. Schäfer and W. Vogelsang, Phys. Rev. Lett. **105**, 252003 (2010).
[44] A. D. Martin, R. G. Roberts, W. J. Stirling and R. S. Thorne, Eur. Phys. J. C **4**, 463 (1998).
[45] E. Leader, A. V. Sidorov and D. B. Stamenov, Phys. Rev. D **82**, 114018 (2010).
[46] V. Blobel *et al.*, Nucl. Phys. **B135**, 379 (1978).
[47] B. Povh and J. Hüfner, Phys. Rev. D **46**, 990 (1992).
[48] L. A. Harland-Lang, A. D. Martin, P. Motylinski and R. S. Thorne, Eur. Phys. J. C **75**, 204 (2015).
[49] S. Alekhin *et al.*, Phys. Rev. D **91**, 094002 (2015).